IIETA International Information and Engineering Technology Association
Advancing the World of Information and Engineering

International Journal of Heat and Technology
Vol. 41, No. 1, February, 2023, pp. 72-86
Journal homepage: http://iieta.org/journals/ijht

The Buoyancy Ratio Number Effect on Al_2O_3-Water Nanofluid Magneto Convective Transport Considering Buongiorno Model in Existence of Surface Radiation

Djelloul Becheri*, Mohammed Douha

Department of Physical Science, High Normal School Teachers of Bechar, B.O.BOX.601 Route de Kenedza, Béchar 08000, Algeria

Corresponding Author Email: becheri.djelloul@ens-bechar.dz

https://doi.org/10.18280/ijht.410108

Received: 8 December 2022
Accepted: 12 February 2023

Keywords:
free convection, Buongiorno model, nanofluid, surface radiation, gauss's theorem

ABSTRACT

A numerical program is adapted for the solution of the 2D, unsteady state equations of coupling convective transport of Buongiorno model and surface radiation; computations are performed in a square cavity differentially heated filled up with an AL_2O_3-water magneto nanofluid. The governing equations in Helmholtz variables (ψ, ω) are solved using a method based on Gauss's theorem integral on triangles meshes. Effects of aiding buoyancy forces (Nr=0.1, 2, and 4), emissivity (ε=0, 0.2, 0.6 and 0.9) on flow structure and convective transport characteristics are investigated. Hartmann number (Ha=50), and Lewis number (Le=5), nanofluids parameter of Brownian motion (Nb=0.5), thermal Rayleigh number (Ra=105), H=0.0098, nanofluids parameter of thermophoretic (Nt=0.5), Prandtl number (Pr=10) are invariable.

1. INTRODUCTION

In recent years, the nanofluids are becoming a popular in many research fields experimentally or numerically to transform base fluids into nanofluid with enhanced thermophysical properties (nanofluid have stronger heat transfer performance than base fluids), such as thermal engineering, solar convection, nuclear industry, biomechanics, etc. By using nanofluids in thermal industrial applications, we can reduce energy consumption and thus preserve the environment more. The nanofluids are prepared by adding a little amount of nanoparticles to a pure fluid (water, ethylene glycol, oil, etc.).

All numerical studies on nanofluids based on pure fluid equations with modified thermal properties, which are obtained by a theoretical or experimental method.

Previously, there was a consensus of researchers on the assumption that slip velocities between the fluid molecules and nanoparticles equals zero at thermal equilibrium, this means the nanofluid have a fixed concentration of nanoparticles, and it is believed that in nanofluids free convection.

By the experimental results of subsequent studies, it was found that the previous assumption is incorrect.

In 2006, the most essential investigation of nanofluids flow and heat transfer done by Buongiorno [1]. Through the calculations he was found that the particle rotation has too small effects on heat transfer enhancement, and refer this enhancement to the effect of Brownian motion and thermophoresis mechanisms, the nanoparticles do not accompany fluid molecules so the nanoparticles concentration not be uniform anymore and we will have a variable volume fraction of the nanofluids.

To explain the observed increase in heat exchange, Buongiorno suggest a model in which the Brownian diffusion effects combined with thermophoresis, a model has been focused on the relative velocity between a nanoparticle and original fluid. He suggested that the absolute velocity of nanoparticle it is the sum of two parts, first part is fluid velocity and the second part is the nanoparticle velocity respect to the fluid (slip velocity). He was able to conclude, the effects of Brownian diffusion and the thermophoresis that will be large when the flow is laminar.

Among the important numerical studies in field of coupling free convection with surface radiation in a square enclosure filled with air the study was made by Akiyama and Chong [2] and Wang et al. [3]. Research in convective transport of nanofluids technologies have had studied in a large number of cavities of different shapes. A number of studies were related to convection in fluids partially or completely confined to solid walls.

Mahmoudi et al. [4] presented a study of natural convection in a square enclosure nanofluid-filled and subjected to the influence of a magnetic field. Mabood et al. [5] presented a radiation effect on Williamson nanofluid flow over a heated surface with magneto hydrodynamics. Rana et al. [6] presented study and analysis of Williamson micropolar of magneto nanofluid flow past stretching sheet. Ibrahim et al. [7] Presented study of free convection inside an inclined enclosure filled with a Ag–water nanofluid and containing a hot solid body (ellipse and circular cylinders) at the center, they used in their studies The COMSOL program as computational tools, They concluded that the Nusselt numbers at the hot left wall is not affected by the change in the value of angle, well they found only at a high Rayleigh number there is effect of the angle on the stream function. Sheikholeslami et al. [8] presented the integrated Brownian motion and thermophoresis effects on free convective transport of nanofluid in an L-shaped cavity; the finite element method was used as method for solving the equations. As a Result, they concluded that the Nusselt number increases with increases in either of the thermal Rayleigh number and the Lewis number but it decreases with increases in either of the aspect ratio and the concentration Rayleigh number. Sheikholeslami et al. [9] Presented MHD effect on free convection treatment in a cavity filled-up with nanofluid, where it was taken into account thermophoresis and Brownian motion effects, the magnet filed is imposed, the Control Volume based Finite Element Method was used to solve the governing equations, They come to a conclusion that it is the Nusselt number is an increasing function of Nr (the buoyancy ratio number) but it is a decreasing function of Hartmann number and Lewis number, they also found that as buoyancy ratio number increases the effects of other active parameters appear larger.

Sheikholeslami [10] presented the electric forces effect on convective transport of Fe_3O_4 nanofluid in a cavity with moving wall, the Control Volume based Finite Element Method was used to solve the governing equations, they come to a conclusion that the existence of coulomb force can change the style of nanofluid flow, and augments the temperature gradient along hot wall. The supplied voltage augment the Nusselt number enhances.

Sheikholeslami and Rokni [11] presented the numerical study of FeO-water nanofluid free convection in a semicircular enclosure subjected to the influence of Lorentz force, the numerical method in which the problem is solved is CVFEM. The results show that the Lorentz force reduces the velocity of the nanofluid and augment the thermal boundary layer thickness, and enhance the heat transfer, Nusselt number is increases with the buoyancy forces but decreases with increasing of Lorentz forces.

Sheikholeslami [12] presented the influence of magnetic field on Fe_3O_4-water nanofluid thermal radiation in a cavity with tilted elliptic inner cylinder, the numerical method in which the problem is solved is CVFEM, the radiation source was adopted in the energy equation ,the conclusion is reached that the Nusselt number goes up with radiation parameter but it goes down with the rise of Lorentz forces.

Sheikholeslami and Rokni [13] presented the effects of magnetic field and thermal radiation on convective transport of Fe_3O_4–H_2O nanofluid, the constant heat flow was imposed for the interior walls as boundary condition, the control volume based finite element method was used to solve the governing equations, the study found that the thermal radiation on convection is more sensible when the buoyancy force is greater, with increasing of radiation parameter, and Hartmann number the thermal boundary layer thickness augments, the nanofluid velocity augments with the rise of radiation parameter.

Sheikholeslami and Shamlooei [14] Magneto hydrodynamic nanofluid flow and convective transport of heat transfer is studied considering thermal radiation, the equations are solved by the control volume-based finite-element method (CVFEM), the rate of heat transfer increases as a function of radiation parameter and Rayleigh number but on contrary, a decrease in heat transfer was recorded with the increasing of Hartmann number. Various papers [15-18], presented the numerical studies on the nanofluid application using Buongiorno model. Various papers [19-26], presented the numerical studies on the nanofluid application.

It is evident through researching in the literature on studies that dealt with the coupling free convection of nanofluids with surface radiation, they are very few, as for the studies that relied specifically on a Buongiorno model coupling with surface radiation, they are rare.

The present work is motivated by this reason, and by all process of natural convection in fact coupled with surface radiation.

The first objective of our present work is to develop a numerical computer code written in FORTRAN language to resolve the two-dimensional, time-dependent convective transport of nanofluid equations coupled with surface radiation based on Buongiorno model inside cavities.

The governing equations are formulated in Helmholtz variables; our numerical computer code is based on a method the basis of which is the application of Gauss's theorem (integrals over a closed line around an area) on a grid made up of triangles.

This numerical computer code can give several advantages for solve several problems of convective transport of nanofluid coupled with surface radiation based on Buongiorno model over complex various geometries, which is difficult with other software.

The second objective of our present work is to use our numerical code as a computational tool to analyze numerical investigation of convective transport of AL_2O_3-water nanofluid coupled with surface radiation based on Buongiorno model in square enclosure differentially heated, where the internal walls considered opaque, diffuse and gray and have the same emissivity value.

Our numerical investigation is concerned with identifying two effects:

The first is the effect of aiding buoyancy forces change, it means the effect of the change of the positive number of buoyancy ratio (Nr=0.1, 2, and 4) in the presence of different values of surface radiation (emissivity ε=0, 0.3, 0.6 and 0.9) on flow structure and convective transport characteristics.

The second is the effect of surface radiation change of cavity internal walls (emissivity ε=0, 0.3, 0.6 and 0.9) on flow structure and convective transport characteristics of nanofluid for different values of Nr (Nr=0.1, 2, and 4).

Hartmann number (Ha=50), and Lewis number (Le=5), nanofluids parameter of Brownian motion (Nb=0.5), thermal Rayleigh number (Ra=10^5), H=0.0098, nanofluids parameter of thermophoretic (Nt=0.5), Prandtl number Pr=10 are invariable.

The main aim of this study is to determine the two effects on the convective transport characteristics of nanofluid in square cavity in the presence of surface radiation and enhances the database of coupled convective transport nanofluid surface radiation.

2. MATHEMATICAL FORMULATION

2.1 Problem description

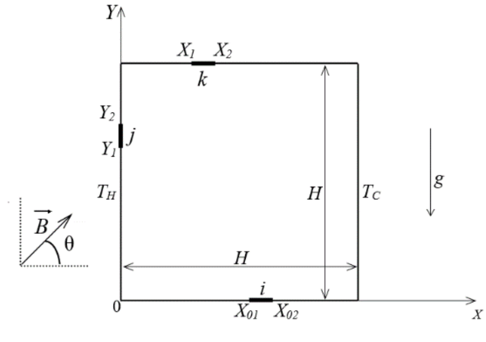

Figure 1. The geometry of studied problem

In this study, we consider a square-shaped enclosure differentially heated that has a shape where the internal walls considered opaque, diffuse and gray and have the same value of emissivity ε, (the schematic diagram is shown in Figure 1). The 2D-dimensional enclosure was filled with AL_2O_3-water nanofluid (Pr=10.0) and the volume fraction of nanoparticle φ_h=0.05 at hot wall. The enclosure walls are subject to condition of no-slip; the standing walls are isothermal at two different temperatures T_C and T_H, while the horizontal walls are considered thermally insulated. We also consider that the boundary conditions applied to nanoparticle volume fraction are identical to the thermal conditions.

The nanofluid inside the cavity is subjected to a fixed magnetic field that creates an angle with the horizon equal to θ=45°.
where the electromagnetic force is given by:

$$\vec{F} = \sigma(\vec{V} \times \vec{B}) \times \vec{B} \tag{1}$$

2.2 Governing equations of nanofluid flow and boundary

2.2.1 Governing equations

The governing equations of nanofluid flow are not change by the presence or absence of surface radiation; also, the isothermal boundary conditions are not affected by the presence or absence of surface radiation. The effect of surface radiation on free convection is done only through the adiabatic thermal conditions in the adiabatic walls. In the absence of radiation the adiabatic condition means that the convective flux is zero in adiabatic wall, while with radiation the adiabatic condition becomes that the sum of the fluxes due to convection and radiation is zero.

The governing equations in nanofluid flow are the conservation equation of mass, tow equations of momentum and, equation of energy and equation of conservation nanoparticles. They are the governing equations of Buongiorno model.

We assumed that the Boussinesq approximation for nanofluid is valid.

$$\rho = \phi\rho_P + (1-\phi)\rho_f \tag{2}$$

$$\rho = \phi\rho_P + (1-\phi)\left\{\rho_{f0}(1-\beta(T-T_c))\right\} \tag{3}$$

where, ρ is the nanofluid's density; ρ_f is the base fluid's density; ρ_P is the nanoparticles's density; ρ_{f0} is the base fluid's density at the reference temperature.

$$\frac{\partial u}{\partial x} + \frac{\partial u}{\partial y} = 0 \tag{4}$$

$$\begin{aligned} &\rho\frac{\partial u}{\partial t^+} + \rho\left(u\frac{\partial u}{\partial x} + v\frac{\partial u}{\partial y}\right) = -\frac{\partial p}{\partial x} + \mu\left(\frac{\partial^2 u}{\partial x^2} + \frac{\partial^2 u}{\partial y^2}\right) \\ &+\kappa B^2(v\sin\lambda\cos\lambda - u\sin^2\lambda) \end{aligned} \tag{5}$$

$$\begin{aligned} &\rho\frac{\partial v}{\partial t^+} + \rho\left(u\frac{\partial v}{\partial x} + v\frac{\partial v}{\partial y}\right) = -\frac{\partial p}{\partial y} + \mu\left(\frac{\partial^2 v}{\partial x^2} + \frac{\partial^2 v}{\partial y^2}\right) \\ &+\kappa B^2(u\sin\theta\cos\theta - v\cos^2\theta) + (\phi-\phi_c)(\rho_P-\rho_f)g \\ &+(1-\phi_c)\rho_f\beta(T-T_c)g \end{aligned} \tag{6}$$

$$\begin{aligned} &\frac{\partial T^+}{\partial t^+} + u\frac{\partial T^+}{\partial x} + v\frac{\partial T^+}{\partial y} = \alpha\left(\frac{\partial^2 T^+}{\partial x^2} + \frac{\partial^2 T^+}{\partial y^2}\right) \\ &+\frac{(\rho c)_P}{(\rho c)_f}\left[\begin{array}{l} D_B\left(\dfrac{\partial\phi}{\partial x}\dfrac{\partial T^+}{\partial x} + \dfrac{\partial\phi}{\partial y}\dfrac{\partial T^+}{\partial y}\right) \\ +\left(\dfrac{D_B}{T_c^+}\right)\left(\left(\dfrac{\partial T^+}{\partial x}\right)^2 + \left(\dfrac{\partial T^+}{\partial y}\right)^2\right) \end{array}\right] \end{aligned} \tag{7}$$

$$\frac{\partial\phi}{\partial t^+} + u\frac{\partial\phi}{\partial x} + v\frac{\partial\phi}{\partial y} = \left[\begin{array}{l} D_B\left(\dfrac{\partial^2\phi}{\partial x^2} + \dfrac{\partial^2\phi}{\partial y^2}\right) \\ +\left(\dfrac{D_T}{T_c^+}\right)\left(\left(\dfrac{\partial T^+}{\partial x}\right)^2 + \left(\dfrac{\partial T^+}{\partial y}\right)^2\right) \end{array}\right] \tag{8}$$

$$\frac{\partial^2\psi^+}{\partial x^2} + \frac{\partial^2\psi^+}{\partial y^2} = -\omega^+ \tag{9}$$

$$u = \frac{\partial\psi^+}{\partial y} \tag{10}$$

$$v = -\frac{\partial\psi^+}{\partial x} \tag{11}$$

The governing equations on variables (ψ, ω) are the equation of mass conservation, vorticity equation, stream function equation and energy equation, equation of nanoparticles conservation.

We used the following non-dimensional variables in order to write the equations in the dimensionless forms:

$$\begin{aligned} &X = \frac{x}{H}, Y = \frac{y}{H}, U = \frac{uH}{\alpha}, V = \frac{vH}{\alpha}, T = \frac{T^+ - T_c^+}{T_h^+ - T_c^+}, \\ &\varphi = \frac{\phi-\phi_c}{\phi_h-\phi_c}, P = \frac{H^2}{\rho\alpha^2}p, \omega = \frac{\omega^+ H^2}{\alpha}, \psi = \frac{\psi^+}{\alpha}, t = \frac{\alpha}{H^2}t^+ \end{aligned} \tag{12}$$

After inserting the dimensionless variables above into governing equations, we can get the following dimensionless system of equation that governs the flow of the nanofluid:

$$\frac{\partial U}{\partial X} + \frac{\partial V}{\partial Y} = 0 \tag{13}$$

$$\begin{aligned} &\frac{\partial\omega}{\partial t} + \left(U\frac{\partial\omega}{\partial X} + V\frac{\partial\omega}{\partial Y}\right) = \Pr\left(\frac{\partial^2\omega}{\partial X^2} + \frac{\partial^2\omega}{\partial Y^2}\right) \\ &+Ha^2\Pr\left(-\frac{\partial V}{\partial Y}\tan\theta + \frac{\partial U}{\partial Y}\tan^2\theta + \frac{\partial U}{\partial X}\tan\theta - \frac{\partial V}{\partial X}\right) \\ &+Ra\Pr\left(\frac{\partial T}{\partial X} + Nr\frac{\partial\varphi}{\partial X}\right) \end{aligned} \tag{14}$$

$$\begin{aligned} &\frac{\partial T}{\partial t} + U\frac{\partial T}{\partial X} + V\frac{\partial T}{\partial Y} = \left(\frac{\partial^2 T}{\partial X^2} + \frac{\partial^2 T}{\partial Y^2}\right) + \\ &Nb\left(\frac{\partial\varphi}{\partial X}\frac{\partial T}{\partial X} + \frac{\partial\varphi}{\partial Y}\frac{\partial T}{\partial Y}\right) + Nt\left(\left(\frac{\partial T}{\partial X}\right)^2 + \left(\frac{\partial T}{\partial Y}\right)^2\right) \end{aligned} \tag{15}$$

$$\left(U\frac{\partial\varphi}{\partial X}+V\frac{\partial\varphi}{\partial Y}\right)=\frac{1}{Le}\left(\frac{\partial^2\varphi}{\partial X^2}+\frac{\partial^2\varphi}{\partial Y^2}\right)+\frac{Nt}{Nb\,Le}\left(\left(\frac{\partial T}{\partial X}\right)^2+\left(\frac{\partial T}{\partial Y}\right)^2\right) \tag{16}$$

$$\frac{\partial^2\psi}{\partial X^2}+\frac{\partial^2\psi}{\partial Y^2}=-\omega \tag{17}$$

$$U=\frac{\partial\psi}{\partial Y} \tag{18}$$

$$V=-\frac{\partial\psi}{\partial X} \tag{19}$$

In the equations above we note the presence of the characteristic numbers, namely the Rayleigh number:

$$Ra=\frac{H^3(1-\phi_c)\rho_f\beta(T_h-T_c)g}{\alpha\mu} \tag{20}$$

The buoyancy ratio number:

$$Nr=\frac{(\phi_h-\phi_c)(\rho_P-\rho_f)}{(1-\phi_c)\rho_f\beta(T_h-T_c)} \tag{21}$$

The Prandtl number:

$$\Pr=\frac{\mu}{\rho\alpha} \tag{22}$$

The Brownian motion parameter:

$$Nb=\frac{(\rho c)_P D_B(\phi_h-\phi_c)}{\alpha(\rho c)_f} \tag{23}$$

The thermophoretic parameter:

$$Nt=\frac{(\rho c)_P D_T(T_h-T_c)^2}{\alpha(\rho c)_f T_c} \tag{24}$$

The Lewis number:

$$Le=\frac{\alpha}{D_B} \tag{25}$$

The Hartman number:

$$Ha=BH\sqrt{\frac{\kappa}{\mu}} \tag{26}$$

Although all the nanofluid flow equation are fully formulated, this system can only be solved by providing values for all the variables at the boundaries of the studied cavity.

2.2.2 Boundary conditions

At all walls:

$$U=V=\psi=0 \tag{27}$$

$$\frac{\partial\psi}{\partial X}=0 \tag{28}$$

$$\omega=-\frac{\partial^2\psi}{\partial X^2}--\frac{\partial^2\psi}{\partial Y^2} \tag{29}$$

At the left isothermal walls:

$$T=\varphi=1 \tag{30}$$

At the right isothermal walls:

$$T=\varphi=0 \tag{31}$$

At the bottom adiabatic walls:

$$\frac{\partial\varphi}{\partial Y}=0 \tag{32}$$

$$-\lambda_{nf}\frac{\partial T}{\partial y}+q_r=0 \tag{33}$$

At the top adiabatic walls:

$$\frac{\partial\varphi}{\partial Y}=0 \tag{34}$$

$$\lambda_{nf}\frac{\partial T}{\partial y}+q_r=0 \tag{35}$$

λ_{nf} is the thermal conductivity of nanofluid which is calculated using a model of Mintsa et al. [26] as follows:

$$\lambda_{nf}=\lambda_f(1.72\varphi+1.0) \tag{36}$$

where, λ_f is the thermal conductivity of water.

q_r is the flux produced by surface radiation and is calculated through the equations:

$$q_r=\frac{\varepsilon}{1-\varepsilon}\left(\sigma T^4-J\right) \tag{37}$$

and J is the vector of radiosity, calculated by the matrix:

$$J=M^{-1}b \tag{38}$$

where,

$$b\left(b_i=\varepsilon\sigma T_i^4\right) \tag{39}$$

is the vector of emissive power and M is the matrix whose elements are written as follows:

$$M_{ij}=\delta_{ij}-(1-\varepsilon)F_{ij} \tag{40}$$

F_{ij} is the view factor of geometry, are calculated through the equations extracted theoretically as follows:

$$F_{ij} = \frac{-1}{2\left(X_{02} - X_{01}\right)}\left[\left.\sqrt{X_{02}^2 + Y^2}\right|_{Y1}^{Y2} - \left.\sqrt{X_{01}^2 + Y^2}\right|_{Y1}^{Y2}\right] \quad (41)$$

$$F_{ik} = \frac{-1}{2\left(X_{02} - X_{01}\right)}\left[\left.\sqrt{\left(X_{02} - X\right)^2 + H^2}\right|_{X1}^{X2} - \left.\sqrt{\left(X_{01} - X\right)^2 + H^2}\right|_{X1}^{X2}\right] \quad (42)$$

So far, we have written each of net radiative flux qr and the radiosity J and adiabatic condition equation on dimensional form, and to write these variables on dimensionless form we used $\sigma(T_H\text{-}T_C)^4$ as reference of J and q_r. After inserting the last dimensionless variable into the equation of the adiabatic boundary conditions, a new dimensionless number appears, which radiation number N_r is where:

$$N_r = \frac{\sigma H (T_H - T_C)^3}{\lambda_{nf}} \quad (43)$$

2.3 Nusselt numbers computation

2.3.1 Nusselt number of convection Nuc

The convective local Nusselt number was calculated locally at each node of the wall with the following expression:

At hot wall:

$$Nuc(y) = -\left(\frac{\partial T}{\partial x}\right)_{x=0} = -\left(\frac{\Delta T}{\Delta x}\right)_{x=0} \quad (44)$$

At cold wall:

$$Nuc(y) = -\left(\frac{\partial T}{\partial x}\right)_{x=H} = -\left(\frac{\Delta T}{\Delta x}\right)_{x=H} \quad (45)$$

Regarding the mean convective local Nusselt number was computed from calculating the average Nusselt number in each wall nodes i as follows:

$$Nuc_{avg} = \frac{\sum_{i=1}^{i=N} Nuc(i)}{N} \quad (46)$$

where, N is the number of nodes in the wall.

2.3.2 Radiative Nusselt number *Nur*

The radiative local Nusselt number was calculated locally at each node of the wall with the following expression:

$$Nur = N_r q_r(y) \quad (47)$$

with

$$N_r = \frac{\sigma H (T_H - T_C)^3}{\lambda} \quad (48)$$

Regarding the mean Nusselt radiative number, we use the same method as calculating the mean Nusselt number for convective:

$$Nur_{avg} = \frac{\sum_{i=1}^{i=N} Nur(i)}{N} \quad (49)$$

3. NUMERICAL CALCULATIONS

In order to numerically calculate the various terms of the governing equation that we obtained earlier, we used the Gauss approach of integrals.

For the numerical calculations of partial derivatives that appear in differential equations, we use the Gauss's theorem, integrals over a closed line around a polygon as shown in Figure 2.

The equation that expresses the Gauss approach is written as follows:

$$\iint_s diva\,ds = \oint_l \vec{n}.a\,dl \quad (50)$$

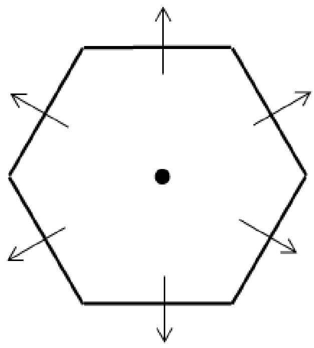

Figure 2. Polygon control volume

where, a the fluxes, s is the total area of the polygon control volume and ds is elemental area, l the total length of the perimeter of the polygon, dl elemental length, $\vec{n}$ is the unit vector perpendicular to dl outward. We can derive from the previous equation and using the unit vector perpendicular components the following approaches:

$$\left(\frac{\partial a}{\partial X}\right) = \frac{1}{s}\int_r a n_X\,dX \text{ and } \left(\frac{\partial a}{\partial Y}\right) = \frac{1}{s}\int_r a n_Y\,dY \quad (51)$$

3.1 Convective flux computation

The convictive flux has been calculated at the polygon centre (see Figure 3) by applying the previously obtained approaches to polygon volume control.

The convictive fluxes are calculated using the two equations:

$$\left(\frac{\partial a}{\partial X}\right)_C = \frac{1}{S_C}\int_{L_C} a n_X\,dX = \frac{1}{S_C}\sum_{i=1}^{NC}\frac{a_{i+1}+a_i}{2}\left(n_X\right)_i\left(X_{i+1}-X_i\right) \quad (52)$$

$$\left(\frac{\partial a}{\partial Y}\right)_C = \frac{1}{S_C}\int_{L_C} a n_Y\,dY = \frac{1}{S_C}\sum_{i=1}^{NC}\frac{a_{i+1}+a_i}{2}\left(n_Y\right)_i\left(Y_{i+1}-Y_i\right) \quad (53)$$

where, S_C is the total polygon surface, a is a flow variable which can be the temperature T, the stream function ψ, Vorticity ω, or temperature, φ nanoparticles traction, (X,Y) coordinates of the vertices of polygon, ($(n_X)_i$, $(n_Y)_i$) are the component of vector $\vec{n}$ on the line segment i and i refers the ordinal number of nodes of the polygon. NC represents the total number of nodes of the polygon.

The integral is calculated along the perimeter of the polygon using the rule of trapezoidal integration for each line segment, so the integral for each line segment is obtained by evaluating the flux averaged value in line segment and use its product with the directed length of line segment.

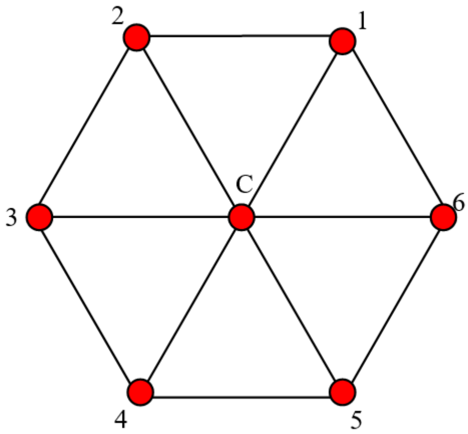

Figure 3. Computation of convictive fluxes at polygon centre

3.2 Diffusive flux computation

The diffusive flux has been calculated at the polygon centre (see Figure 4), Since we have the fluxes values in the all grid nodes (T, ψ, ω, φ), to calculate the diffusive flux, we are required to design inner polygons; we designed the inner polygons as shown in the figure below, the desired goal of these inner polygons is to calculate the first-order derivatives in the middle of the inner polygons line segment.

The diffusive fluxes are calculated using the two equations:

$$\left(\frac{\partial^2 a}{\partial X^2}\right)_C = \left(\frac{\partial}{\partial X}\left(\frac{\partial a}{\partial X}\right)\right)_C = \frac{1}{S_{CI}}\int_{L_{CI}}\left(\frac{\partial a}{\partial X}\right)n_X\,dX = \frac{1}{S_{CI}}\sum_{i=1}^{NC}\left(\frac{\partial a}{\partial X}\right)_{i+1/2}(n_X)_i\,(X_{i+1}-X_i) \tag{54}$$

$$\left(\frac{\partial^2 a}{\partial Y^2}\right)_C = \left(\frac{\partial}{\partial Y}\left(\frac{\partial a}{\partial Y}\right)\right)_C = \frac{1}{S_{CI}}\int_{L_{CI}}\left(\frac{\partial a}{\partial Y}\right)n_Y\,dY = \frac{1}{S_{CI}}\sum_{i=1}^{NC}\left(\frac{\partial a}{\partial Y}\right)_{i+1/2}(n_Y)_i\,(Y_{i+1}-Y_i) \tag{55}$$

where, S_{CI} is the total inner polygon surface, a is a flow variable (the temperature T, the stream function ψ, Vorticity ω, or temperature, φ nanoparticles traction), (X,Y) coordinates of the vertices of inner polygon, ($(n_X)_i$, $(n_Y)_i$) are the component of vector $\vec{n}$ on the line segment i and i refers the ordinal number of nodes of the polygon, (i+1/2) is the centre of inner polygon line segment, NC represents the total number of nodes of the polygon.

Since the centre of the line segment of inner polygon is congruent with the centre of parallelogram as shown in Figure 5, we chose to apply on the parallelogram area the same approaches used previously to calculate the first-order derivative fluxes, so that the derivates at middle line segment of inner polygon is the sum of four terms.

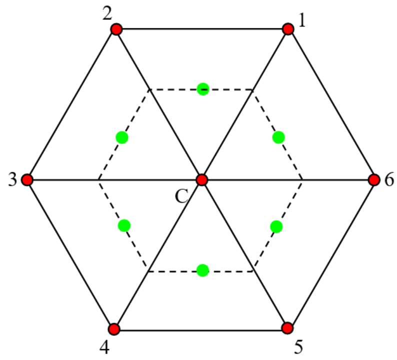

Figure 4. Computation of diffusive fluxes at polygon centre

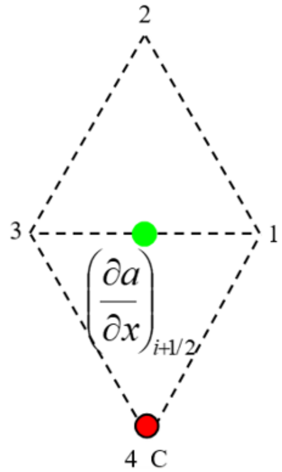

Figure 5. Computation of the first -order derivatives at parallelogram centre

The first-order derivatives at the parallelogram centre are calculated by:

$$\left(\frac{\partial a}{\partial X}\right)_{i+1/2} = \frac{1}{S_d}\int_{L_d} a n_X\,dX = \frac{1}{S_d}\sum_{j=1}^{4}\frac{a_{j+1}+a_j}{2}(n_X)_j\left(X_{j+1}-X_j\right) \tag{56}$$

$$\left(\frac{\partial a}{\partial Y}\right)_{i+1/2} = \frac{1}{S_d}\int_{L_d} a n_Y\,dY = \frac{1}{S_d}\sum_{j=1}^{4}\frac{a_{j+1}+a_j}{2}(n_Y)_j\left(Y_{j+1}-Y_j\right) \tag{57}$$

where, S_d is the total parallelogram surface, a is a flow variable (the temperature T, the stream function ψ, Vorticity ω, or temperature, φ nanoparticles traction), (X,Y) coordinates of the vertices of inner polygon, j represents to the number of four ordered nodes of the parallelogram and ($(n_X)_i$, $(n_Y)_i$) are the component of vector $\vec{n}$ on the line segment i and i refers the ordinal number of nodes of the polygon, (i+1/2) is the centre of inner polygon line segment, NC represents the total number of nodes of the polygon.

4. RESULT AND DISCUSSION

4.1 Validation

Before adopting our numerical code to study our model, we have selected some studies closest to our models for validating our code, among the studies that compared the results of our numerical code with their results were studies prepared by Akiyama and Chong [2] and Wang et al. [3].

Table 1. Comparison of our average Nusselt numbers of isothermals walls with the numbers of Wang et al. [3]

H=0.045, T_O=293.5K, ΔT=10K, Ra=10^5						
Result	**Coldwall**			**Hotwall**		
	Nuc	Nur	Nuc+ Nur	Nuc	Nur	Nuc+Nur
[3], ε=0.0	*4.540*	0	*4.540*	*4.540*	0	*4.540*
Our result, ε=0.0	*4.553*	0	*4.553*	*4.552*	0	*4.552*
Error	*0.28%*	*0%*	*0.28%*	*0.26%*	*0%*	*0.26%*
[3], ε=0.2	*4.394*	*1.090*	*5.484*	*4.411*	*1.073*	*5.484*
Our result ε=0.2	*4.413*	*1.089*	*5.502*	*4.430*	*1.072*	*5.502*
Error	*0.43%*	*0.09%*	*0.32%*	*0.42%*	*0.09%*	*0.32%*
[3], ε=0.8	*4.189*	*5.196*	*9.385*	*4.247*	*5.137*	*9.384*
Our result ε=0.8	*4.200*	*5.198*	*9.398*	*4.259*	*5.139*	*9.398*
Error	*0.26%*	*0.03%*	*0.13%*	*0.28%*	*0.03%*	*0.14%*

A study of coupling of free convection with surface radiation in a square enclosure air-filled, so that all its walls have the same value of emissivity.

Table 1 shows a comparison of our average Nusselt numbers of isothermals walls with the numbers of Wang et al. [3]. What can be observed is the largely congruence between the results of our automated program and the results of the study [3].

4.2 Effects of active parameters

It is necessary to note that negative Nr values (opposing buoyancy forces) appear more complex due to inconsistent flow patterns, so in this study, the results for auxiliary buoyancy forces (positive Nr), where is the temperature and species induced buoyancy pushing in same direction, that is, due to the compatibility of the two flow patterns.

The Figure 6 and 7 illustrates the influence of surface radiation and the species-induced buoyancy force on the isotherms lines and flow structure for different buoyancy ratio numbers and for the different emissivity values. We can see for the isotherms lines the effects are visible especially near along the horizontal walls, regarding the effects on the flow structure the stream function lines tend to become square and converge to each other especially along the isothermal walls with the increase of Nr buoyancy ratio number.

Figure 8 (left) shows the net radiative flux distribution and (right) shows the temperature distribution on the horizontal walls for different emissivity values and at different Nr number. Figure 9 (left) shows temperature distribution and (right) the profiles of horizontal velocity at vertical median line x=0.5 for different emissivity values and for different Nr number.

The average net radiative flux of the upper wall is positive; while for the lower wall is negative (the upper wall loses heat by radiation, while the lower wall acquires heat by radiation).

We can see at the top adiabatic wall the average net radiative flux increases with the increase in emissivity value, the top horizontal wall loses more heat, For the bottom adiabatic wall the average net radiative flux decreases with the increase in the emissivity value, the bottom adiabatic wall gains more heat.

Despite the significant changes in the net radiative flux value of horizontal walls, the temperature decrease of the upper horizontal wall and the temperature increase of the lower horizontal wall is small, and since the adiabatic condition in the horizontal walls is expressed mathematically as the sum of the convective and radiative flux is zero.

The explanation for the small changes observed in temperatures of the horizontal wall is due to the large value of the thermal conductivity of the nanofluid, unlike what is found in previous studies on the effect of surface radiation when the fluid used is air which has a small thermal conductivity, where we find a significant decrease in the temperature of the top wall, as well as a significant increase in the temperature of the bottom wall.

It can be noted that the increase in emissivity leads to a slight decrease of nanofluid temperature near the upper adiabatic wall and a slight increase of nanofluid temperature near the bottom adiabatic wall, these slight changes recorded in the nanofluid temperature cause a slight rise in the horizontal velocity in the vicinity of the horizontal walls.

Figure 10 (left) shows the temperature profiles at x=0.5 and (right) shows the temperature on the horizontal walls for different Nr values and for (1) ε=0.0, (2) ε=0.3, (3) ε=0.6 and (4) ε=0.9.

We can see the increasing of species-induced buoyancy force heats up the top adiabatic wall and cools down the bottom adiabatic wall with the increasing of buoyancy ratio number.

This behaviour of the horizontal wall temperature is caused by the fact that the upper wall gains heat while the lower wall loses heat, this is due to the increase in heat transfer from the hot wall to the top wall and from the cold wall to the bottom wall with the increase of the number of nanoparticles in nanofluid.

We can see also that the nanofluid in the upper half of cavity is heat up but in the other half cools dawn with the increasing of species-induced buoyancy force (the increasing of Nr) especially near the adiabatic walls; this is due to the temperature change in the horizontal wall.

Figure 11 shows the horizontal velocity profiles at x=0.5 for (1) ε=0.0, (2) ε=0.3, (3) ε=0.6 and (4) ε=0.9 and for different values of buoyancy ratio number Nr. It is noted that near along the horizontal walls the horizontal velocity is increased with the increasing of Nr but in the cavity core the horizontal velocity is slightly decreased.

Figure 12 shows the curve change for average Nusselt number of convections of active walls in terms of Nr the buoyancy ratio number for different emissivity.

We notice that the average Nusselt numbers of convection increases clearly with the increasing of Nr; this is due to the increase in heat transfer process due to the increase of the nanoparticles number in the nanofluid, as the nanofluid reaches hotter to the cold wall and reaches colder to the hot wall.

Figure 13 shows the curve change for average Nusselt number of convections of active walls in terms of emissivity for different Nr values (the buoyancy ratio number).

In general, we notice a slight decrease in the average Nusselt numbers of convection with the increasing of emissivity; this is due to the decrease in heat transfer process due to the slight change in the temperature of the horizontal walls, as the nanofluid reaches hotter to the hot wall and reaches colder to the cold wall.

Figure 14 shows the curve change for average Nusselt number of radiation of active walls in terms of emissivity; we notice that the average Nusselt numbers of radiation increases clearly with the increasing of emissivity.

This is due to the fact that the Nusselt number of radiation is directly proportional to emissivity.

Figure 15 shows the curve change for average Nusselt number of radiation of active walls in terms of Nr the buoyancy ratio number, we notice a slight increase in the average Nusselt numbers of radiation with the increasing of Nr; this is due to the slight change in the horizontal walls temperature.

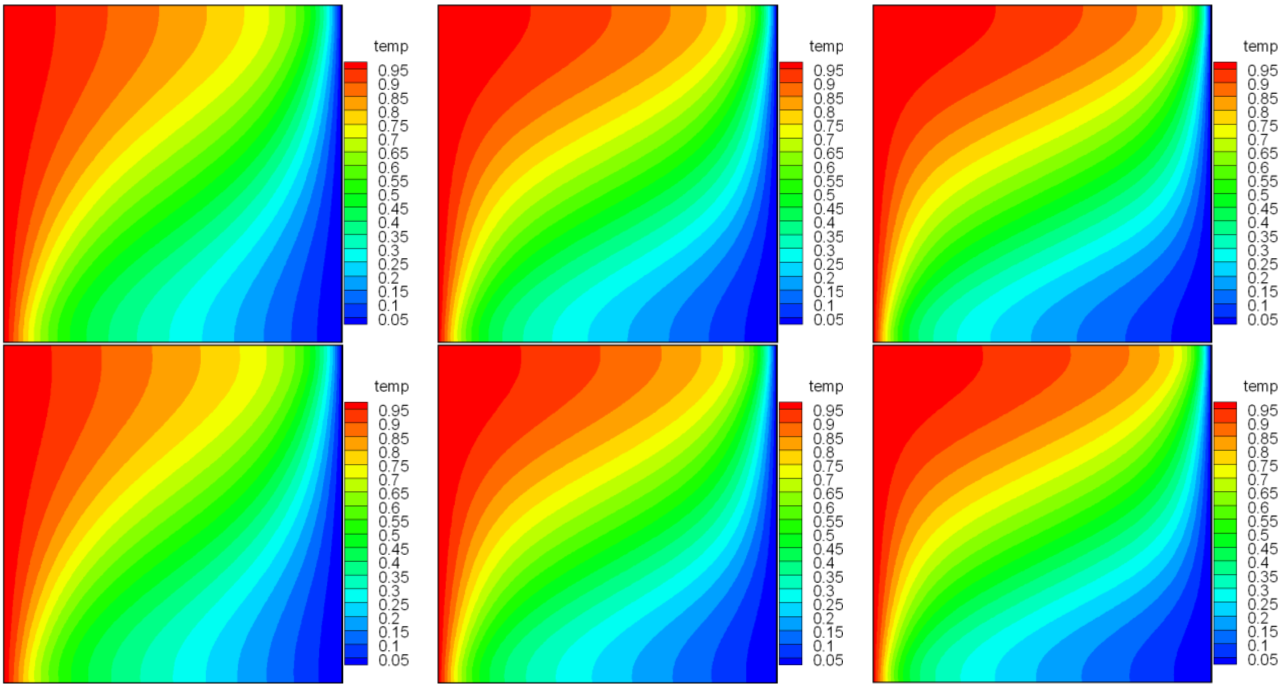

(1)

(2)

(a) (b) (c)

Figure 6. Isotherms for (a) Nr=0.1, (b) Nr=2, (c) Nr=4 and at the emissivity equals (1) ε=0.0, (2) ε=0.6

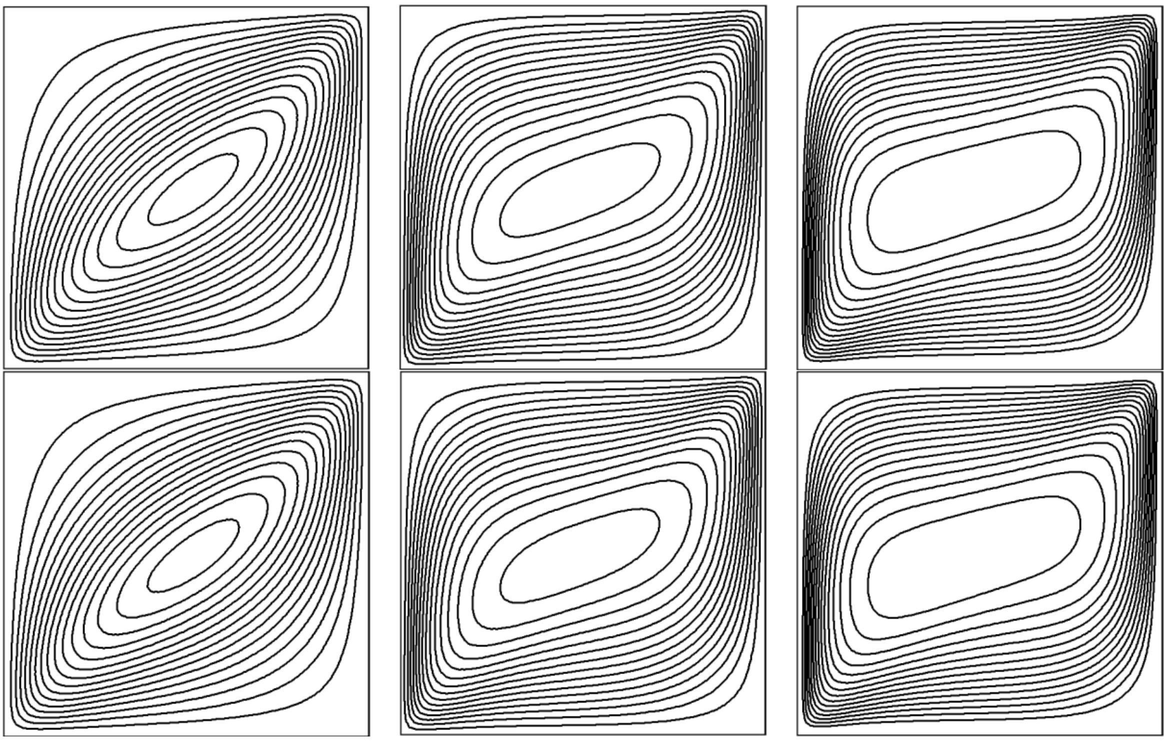

(1)

(2)

(a) (b) (c)

Figure 7. The flow structure for (a) Nr=0.1, (b) Nr=2, (c) Nr=4 and at the emissivity equals (1) ε=0.3 and (2) ε=0.9

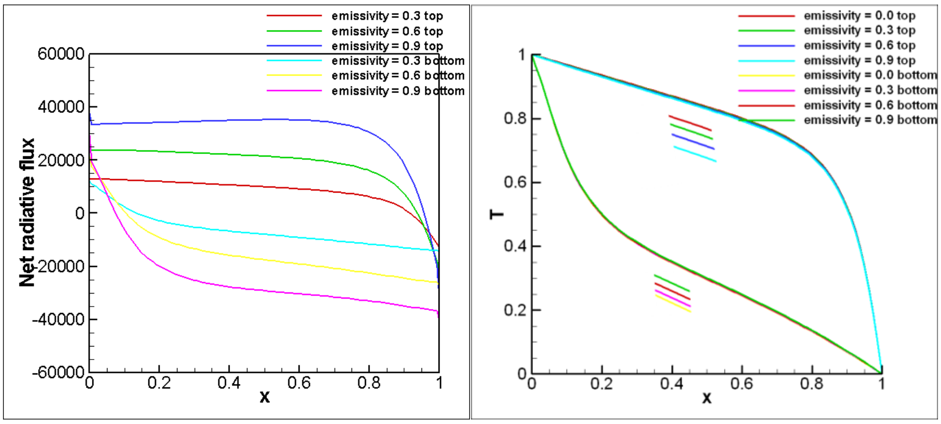

(a)

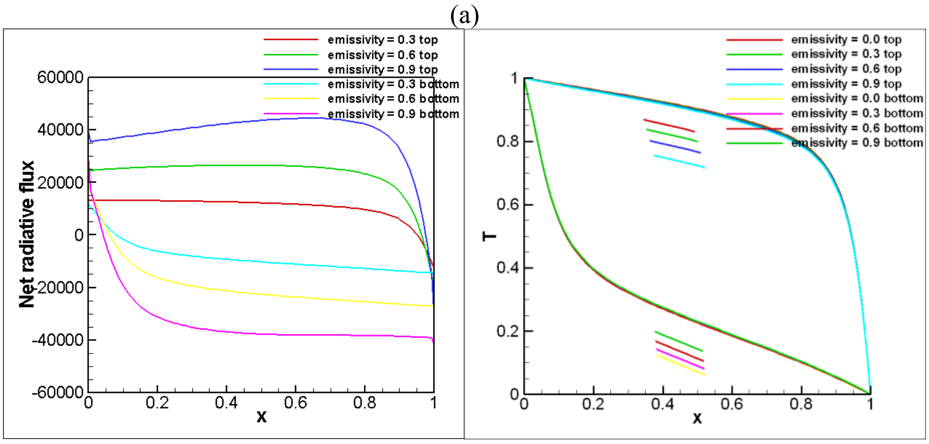

(b)

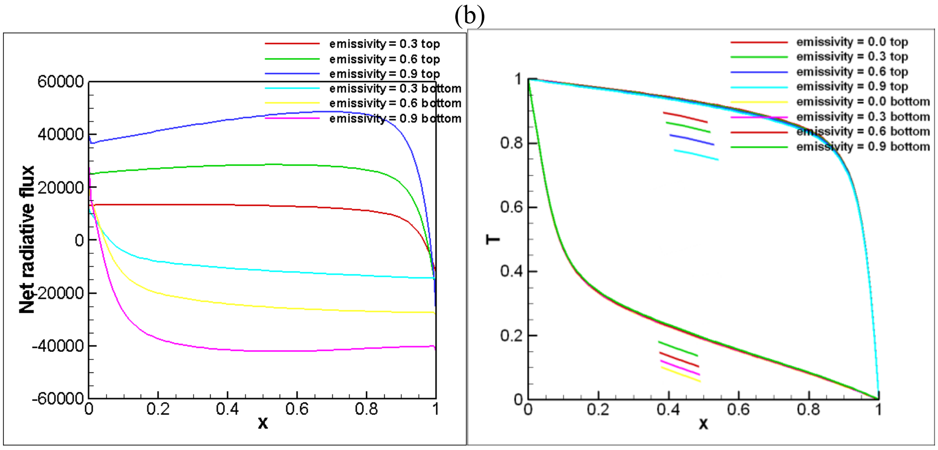

(c)

Figure 8. The flux of net radiative (left) and the temperature (right) at the adiabatic walls at (a) Nr=0.1, (b) Nr=2, (c) Nr=4 and for different emissivity values

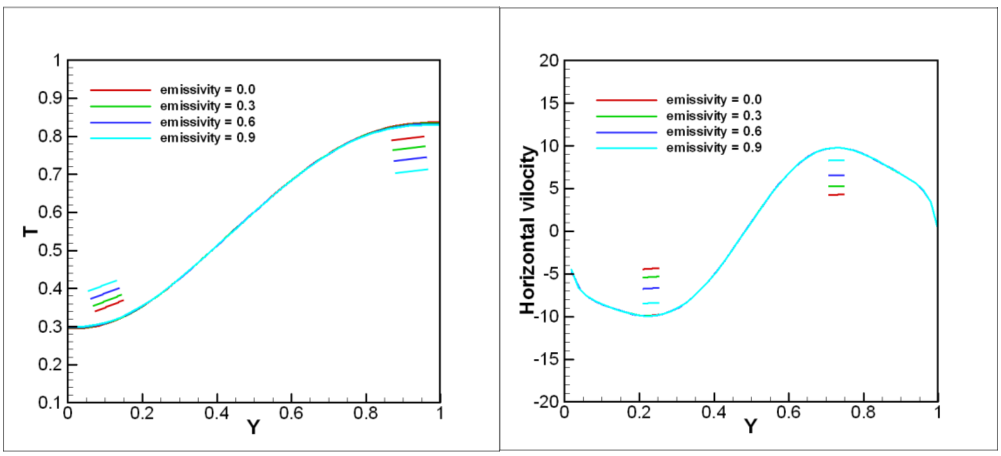

(a)

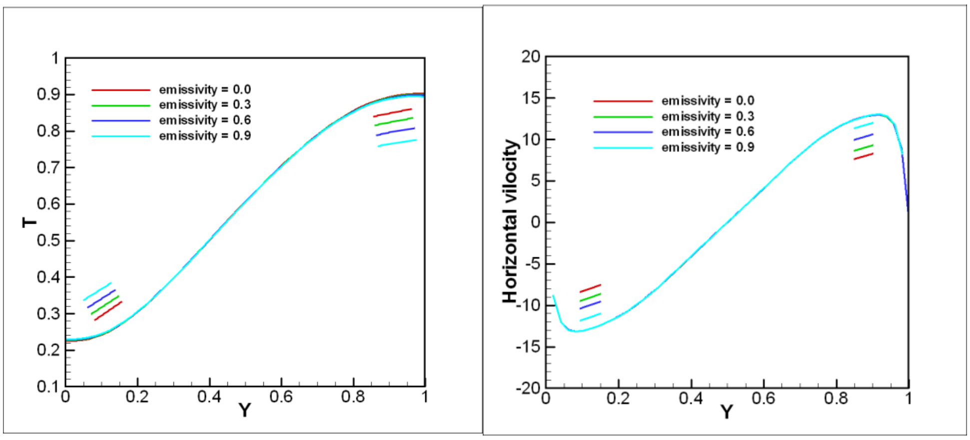

(b)

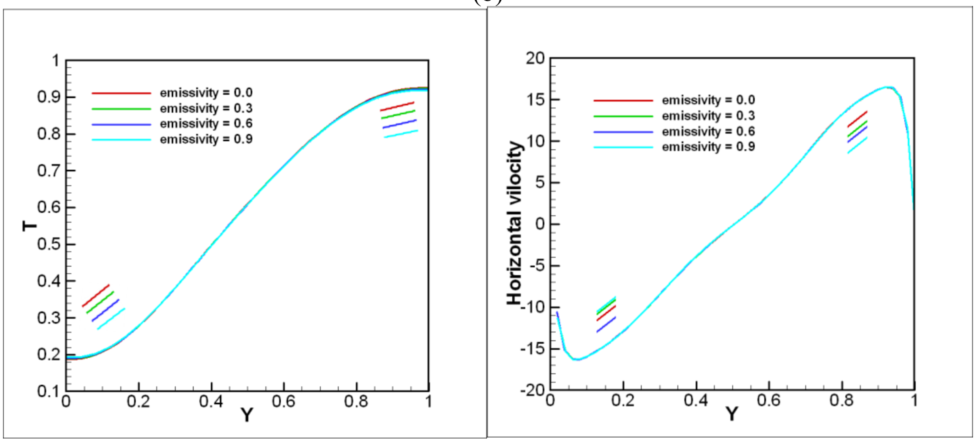

(c)

Figure 9. Temperature (left), profiles of horizontal velocity on x=0.5 (right) at (a) Nr=0.1, (b) Nr=2, (c) Nr=4 and for different emissivity values

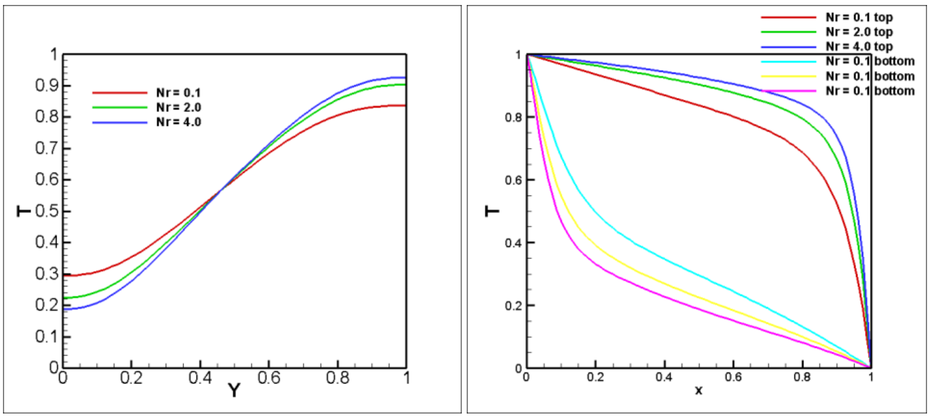

(1)

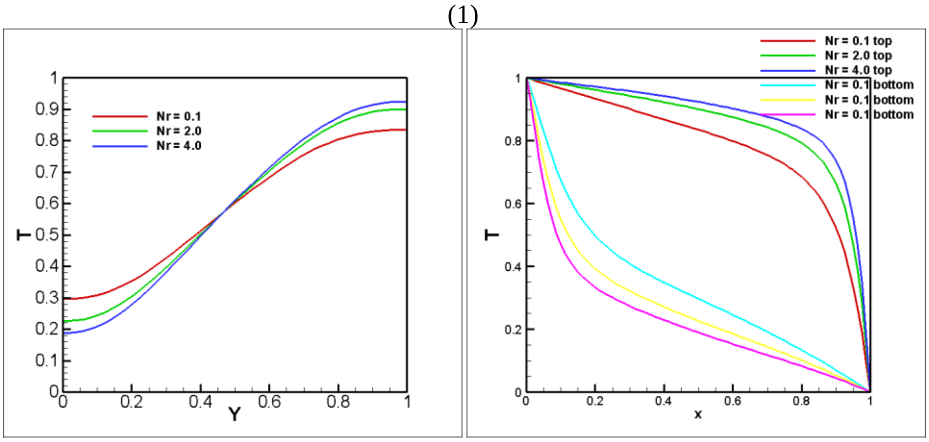

(2)

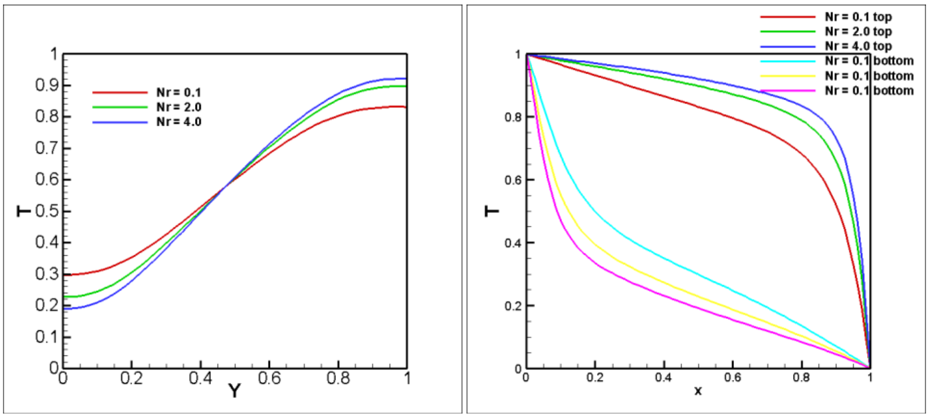

(3)

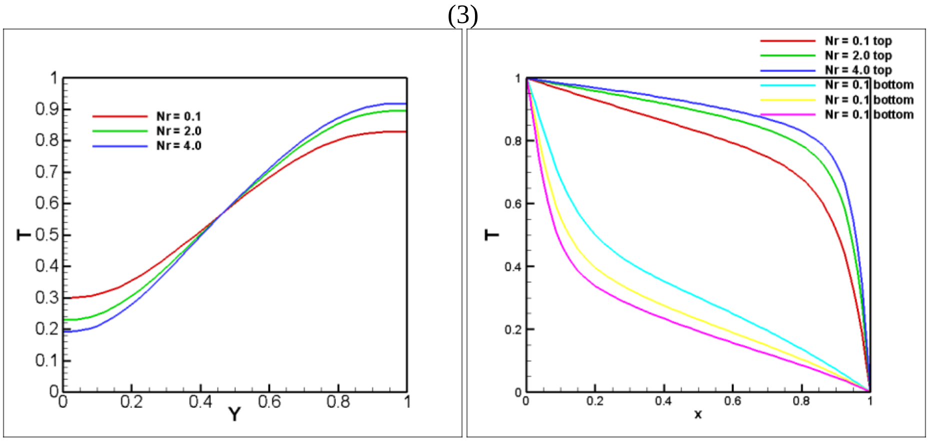

(4)

Figure 10. Temperature profiles at x=0.5 (left) and Temperature on the horizontal walls (right) at (1) ε=0.0, (2) ε=0.3, (3) ε=0.6 and (4) ε=0.9 and for different values of buoyancy ratio number

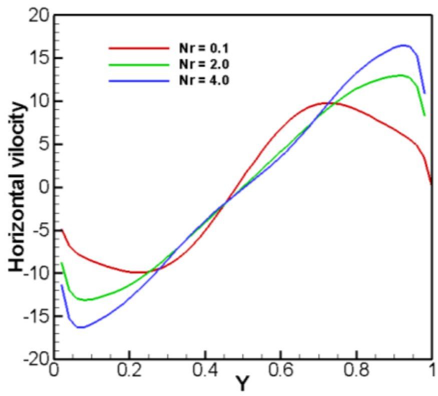

(1)

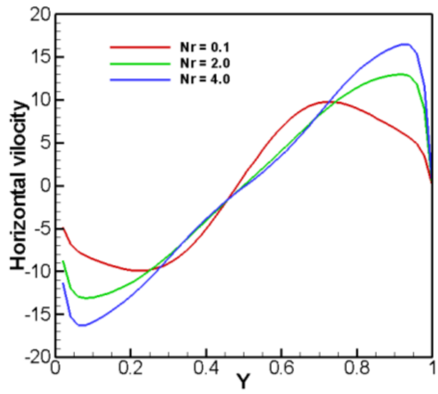

(2)

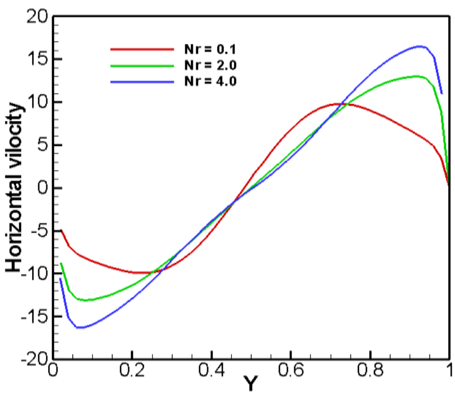

(3)

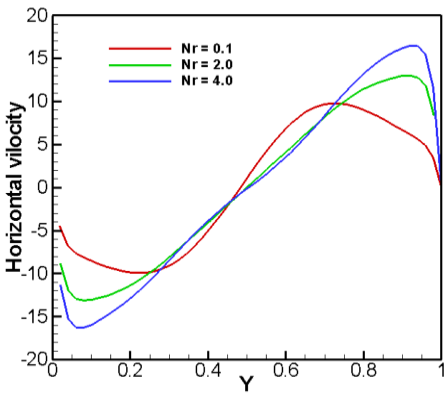

(4)

Figure 11. The profiles of horizontal velocity on x=0.5 at (1) ε=0.0, (2) ε=0.3, (3) ε=0.6 and (4) ε=0.9 and for different values of Nr the buoyancy ratio number

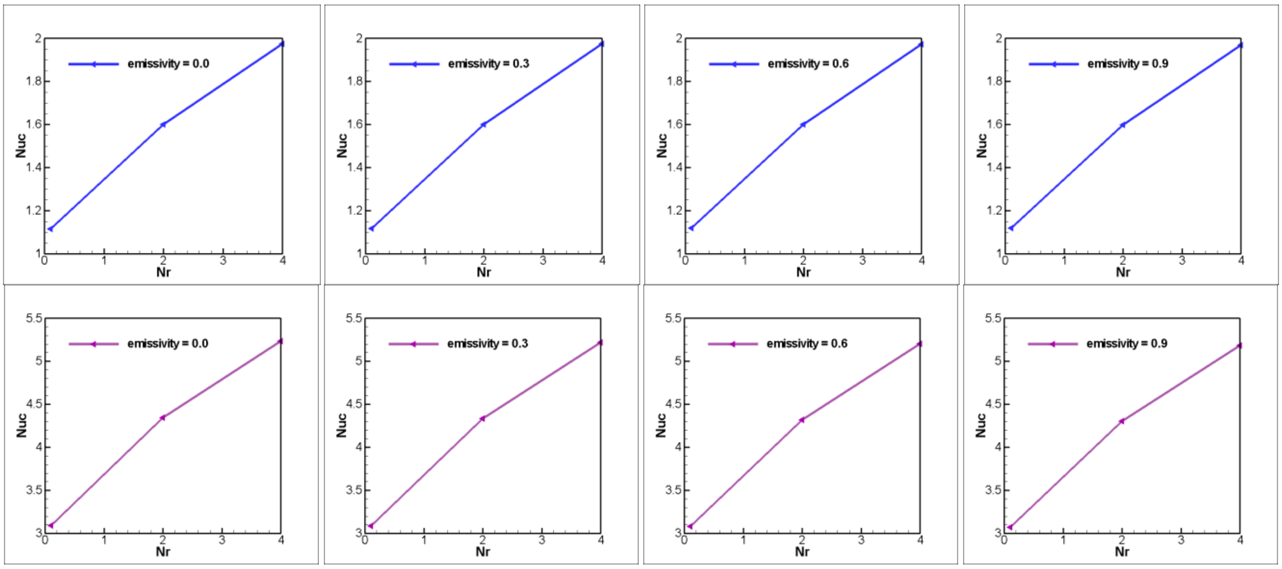

Figure 12. The curve change for average Nusselt number of convection in terms of Nr the buoyancy ratio number at (above) hot wall (below) cooled wall

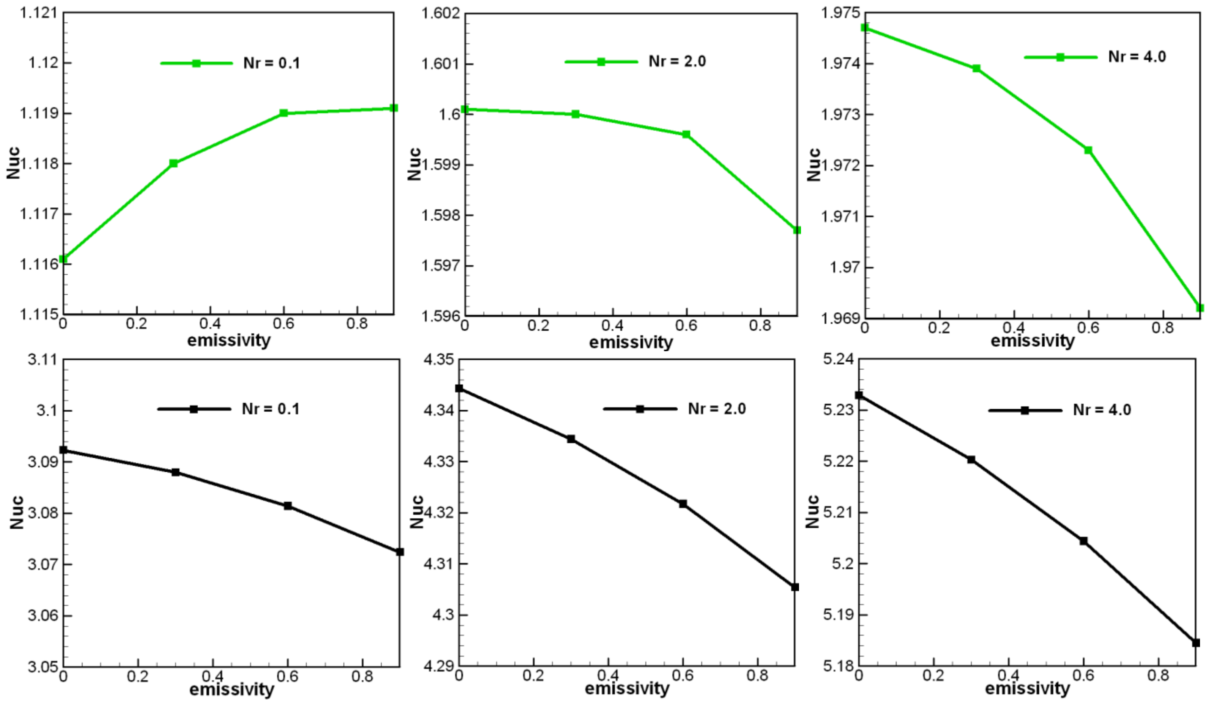

Figure 13. The curve change for average Nusselt number of convection in terms of emissivity at (above) hot wall (below) cooled wall

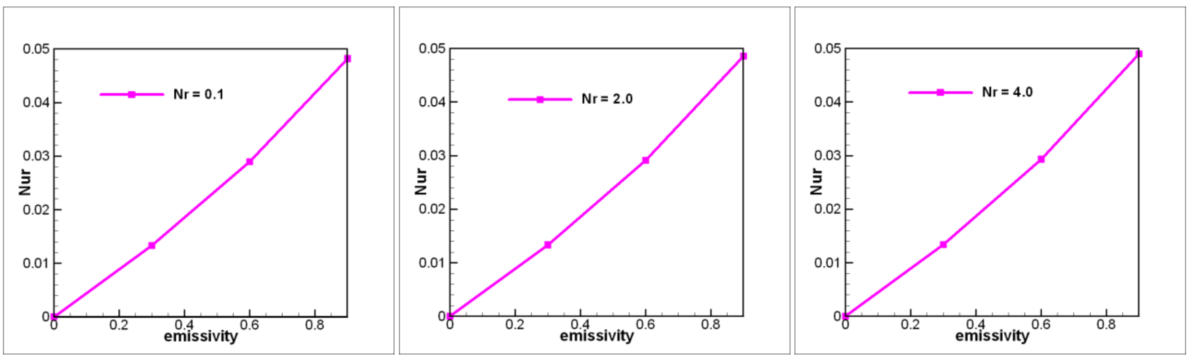

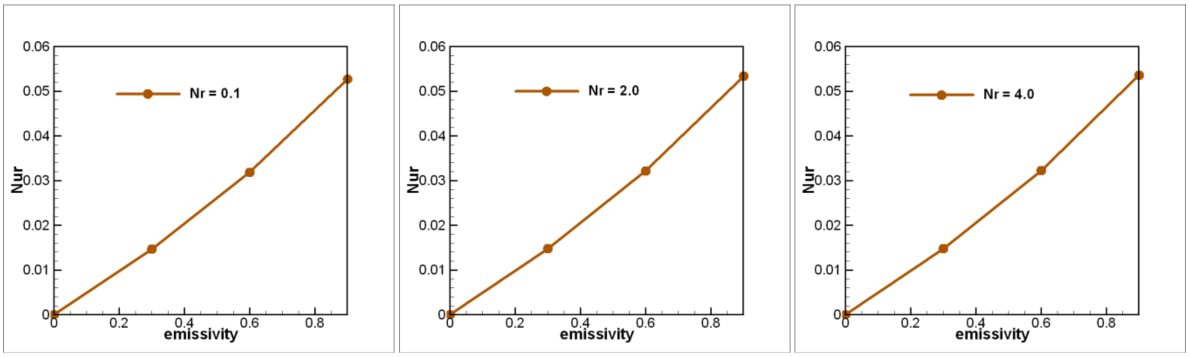

Figure 14. The curve change for average Nusselt number of radiation in terms of emissivity at (above) hot wall (below) cooled wall

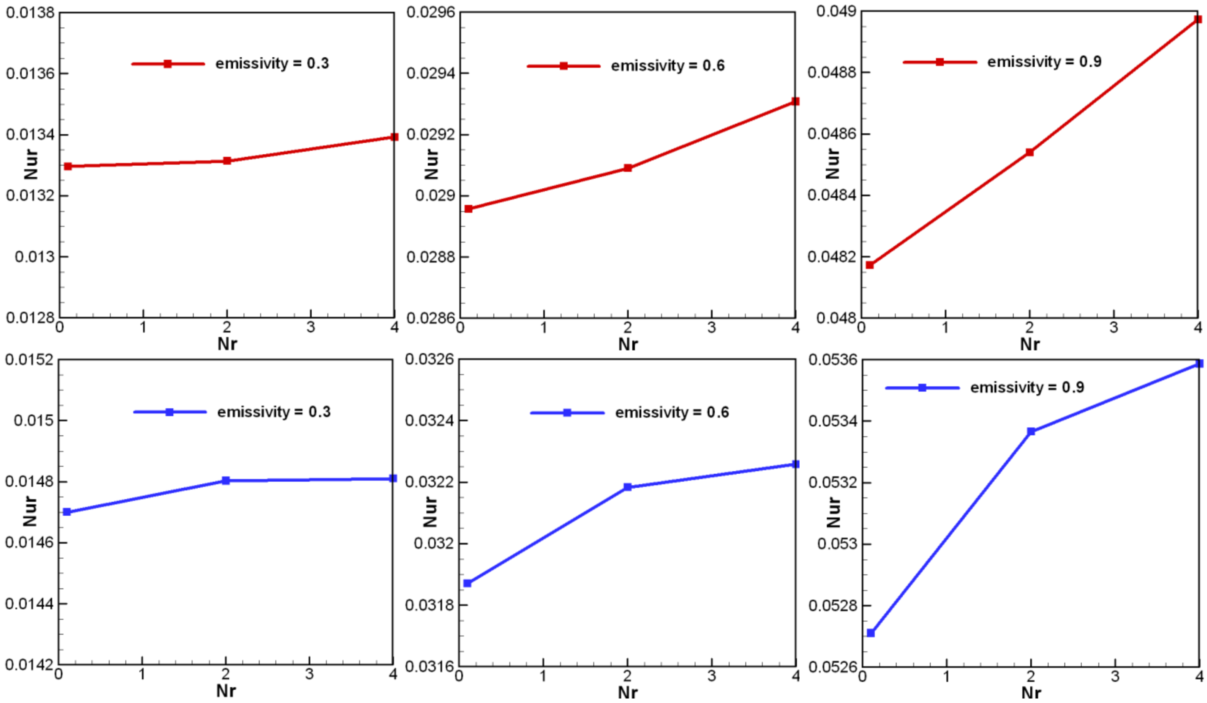

Figure 15. The curve change for average Nusselt number of radiation in terms of Nr the buoyancy ratio number at (above) hot wall (below) cooled wall

5. CONCLUSIONS

Convective transport coupling with Surface radiation in AL_2O_3-water nanofluid-filled square room has been investigated numerically by using Buongiorno model.

We have written a computer code for a method that uses Gauss's theorem integrals, this code was developed for use on triangles meshes.

Our numerical code validated its results by comparing them with the result of previous studies.

This program has ability to solve several flow fields problem, even in complex geometries.

The current numerical investigation showed that the flow and heat field's characteristics were affected by emissivity and species-induced buoyancy force. The species-induced forces (the buoyancy ratio number Nr) clearly affect the isotherms lines and the flow structure especially near the adiabatic walls, while hardly any effect of emissivity is seen on them.

In general, with all fluids, the heat transfer decreases with the increasing of emissivity value of walls (the decreasing of convective Nusselt number of active wall), and this is due to the fact that with the increasing of emissivity, the temperature differences of cavity walls decrease, with more precisely, the temperature difference of adiabatic walls decreases.

Through our study, the effect of the increasing of emissivity value of walls on decreasing of heat transfer is small when there is a fluid with a large thermal conductivity inside the cavity (nonofluid for example), on the contrary, if inside the cavity there is a fluid with a small thermal conductivity such as air, the effect of increasing the emissivity value of the walls will be greater.

That is, the thermal conductivity of fluid is what determines the extent to which the influence of the increasing of emissivity value of walls, the large thermal conductivity of fluid inside the cavity, the less effect of the increasing of emissivity value of walls.

Since increasing of the Nr value (the buoyancy ratio number) increases the value of thermal conductivity of nanofluid, the increasing of Nr reduces the effect of the increasing of emissivity value of walls.

The increasing of species-induced buoyancy force (the increasing of Nr=the increasing of nanoparticles number) increase the heat transfer clearly (the increase of convective Nusselt number of active walls).

The effect of the increasing of species-induced buoyancy force (the increasing of Nr=the increasing of nanoparticles number) with surface radiation is similar to the case without surface radiation.

REFERENCES

[1] Buongiorno, J. (2006). Convective transport in nanofluids. ASME Journal of Heat and Mass Transfer, 128(3): 240-250. http://dx.doi.org/10.1115/1.2150834

[2] Akiyama, M., Chong, Q.P. (1997). Numerical analysis of natural convection with surface radiation in a square enclosure. Numerical Heat Transfer, Part A Applications, 32(4): 419-433. http://dx.doi.org/10.1080/10407789708913899

[3] Wang, H., Xin, S., Le Quéré, P. (2006). Étude numérique du couplage de la convection naturelle avec le rayonnement de surfaces en cavité carrée remplie d'air. Comptes Rendus Mécanique, 334(1): 48-57. http://dx.doi.org/10.1016/j.crme.2005.10.011

[4] Mahmoudi, A., Mejri, I., Omri, A. (2016). Study of natural convection in a square cavity filled with nanofluid and subjected to a magnetic field. International Journal of Heat and Technology, 34(1): 73-79. http://dx.doi.org/10.18280/ijht.340111

[5] Mabood, F., Ibrahim, S.M., Lorenzini, G., Lorenzini, E. (2017). Radiation effects on Williamson nanofluid flow over a heated surface with magnetohydrodynamics. International Journal of Heat and Technology, 35(1): 196-204. http://dx.doi.org/10.18280/ijht.350126

[6] Rana, B.M.J., Arifuzzaman, S.M., Reza-E-Rabbi, S., Ahmed, S.F., Khan, M.S. (2019). Energy and magnetic flow analysis of Williamson micropolar nanofluid through stretching sheet. International Journal of Heat and Technology, 37(2): 487-496. http://dx.doi.org/10.18280/ijht.370215

[7] Ibrahim, M.N.J., Hammoodi, K.A., Abdulsahib, A.D., Flayyih, M.A. (2022). Study of natural convection inside inclined nanofluid cavity with hot inner bodies (circular and ellipse cylinders). International Journal of Heat and Technology, 40(3): 699-705. http://dx.doi.org/10.18280/ijht.400306

[8] Sheikholeslami, M., Chamkha, A.J., Rana, P., Moradi, R. (2017). Combined thermophoresis and Brownian motion effects on nanofluid free convection heat transfer in an L-shaped enclosure. Chinese Journal of Physics, 55(6): 2356-2370. http://dx.doi.org/10.1016/j.cjph.2017.09.011

[9] Sheikholeslami, M., Gorji-Bandpy, M., Ganji, D.D., Rana, P., Soleimani, S. (2014). Magnetohydrodynamic free convection of Al_2O_3–water nanofluid considering Thermophoresis and Brownian motion effects. Computers & Fluids, 94: 147-160. http://dx.doi.org/10.1016/j.compfluid.2014.01.036

[10] Sheikholeslami, M. (2017). Influence of Coulomb forces on Fe_3O_4–H_2O nanofluid thermal improvement. International Journal of Hydrogen Energy, 42(2): 821-829. http://dx.doi.org/10.1016/j.ijhydene.2016.09.185

[11] Sheikholeslami, M., Rokni, H.B. (2017). Numerical modeling of nanofluid natural convection in a semi annulus in existence of Lorentz force. Computer Methods in Applied Mechanics and Engineering, 317: 419-430. http://dx.doi.org/10.1016/j.cma.2016.12.028

[12] Sheikholeslami, M. (2017). Magnetic field influence on nanofluid thermal radiation in a cavity with tilted elliptic inner cylinder. Journal of Molecular Liquids, 229: 137-147. http://dx.doi.org/10.1016/j.molliq.2016.12.024

[13] Sheikholeslami, M., Rokni, H.B. (2017). Magnetic nanofluid natural convection in the presence of thermal radiation considering variable viscosity. The European Physical Journal Plus, 132: 1-12. http://dx.doi.org/10.1140/epjp/i2017-11498-4

[14] Sheikholeslami, M., Shamlooei, M. (2017). Fe_3O_4–H_2O nanofluid natural convection in presence of thermal radiation. International Journal of Hydrogen Energy, 42(9): 5708-5718. https://doi.org/10.1080/10407782.2015.1125709

[15] Turkyilmazoglu, M. (2021). On the transparent effects of Buongiornonano fluid model on heat and mass transfer. The European Physical Journal Plus, 136(4): 1-15. http://dx.doi.org/10.1140/epjp/s13360-021-01359-2

[16] Khan, M., Ahmed, A., Ahmed, J. (2020). Transient flow of magnetized Maxwell nanofluid: Buongiorno model perspective of Cattaneo-Christov theory. Applied Mathematics and Mechanics, 41: 655-666. http://dx.doi.org/10.1007/s10483-020-2593-9

[17] Rajput, S., Verma, A.K., Bhattacharyya, K., Chamkha, A.J. (2021). Unsteady nonlinear mixed convective flow of nanofluid over a wedge: Buongiorno model. Waves in Random and Complex Media, 1-15. https://doi.org/10.1016/j.csite.2020.100820

[18] Dawar, A., Shah, Z., Tassaddiq, A., Kumam, P., Islam, S., Khan, W. (2021). A convective flow of Williamson nanofluid through cone and wedge with non-isothermal and non-isosolutal conditions: A revised Buongiorno model. Case Studies in Thermal Engineering, 24: 100869. https://doi.org/10.1016/j.csite.2021.100869

[19] Sheikholeslami, M. (2018). Magnetic source impact on nanofluid heat transfer using CVFEM. Neural Computing and Applications, 30: 1055-1064.https://doi.org/10.1007/s00521-016-2740-7

[20] Sheikholeslami, M., Vajravelu, K.J.A.M. (2017). Nanofluid flow and heat transfer in a cavity with variable magnetic field. Applied Mathematics and Computation, 298: 272-282. http://dx.doi.org/10.1016/j.amc.2016.11.025

[21] Sheikholeslami, M., Hayat, T., Alsaedi, A. (2017). RETRACTED: Numerical simulation of nanofluid forced convection heat transfer improvement in existence of magnetic field using lattice Boltzmann method. International Journal of Heat and Mass Transfer, 108: 1870-1883. http://dx.doi.org/10.1016/j.ijheatmasstransfer.2017.01.044

[22] Sheikholeslami, M., Vajravelu, K., Rashidi, M.M. (2016). Forced convection heat transfer in a semi annulus under the influence of a variable magnetic field. International Journal of Heat and Mass Transfer, 92: 339-348. http://dx.doi.org/10.1016/j.ijheatmasstransfer.2015.08.066

[23] Sheikholeslami, M., Ellahi, R. (2015). Three dimensional mesoscopic simulation of magnetic field effect on natural convection of nanofluid. International Journal of Heat and Mass Transfer, 89: 799-808.

http://dx.doi.org/10.1016/j.ijheatmasstransfer.2015.05.110

[24] Sheikholeslami, M., Hayat, T., Alsaedi, A., Abelman, S. (2017). Numerical analysis of EHD nanofluid force convective heat transfer considering electric field dependent viscosity. International Journal of Heat and Mass Transfer, 108: 2558-2565. http://dx.doi.org/10.1016/j.ijheatmasstransfer.2016.10.099

[25] Sheikholeslami, M., Chamkha, A.J. (2016). Electrohydro dynamic free convection heat transfer of a nanofluid in a semi-annulus enclosure with a sinusoidal wall. Numerical Heat Transfer, Part A: Applications, 69(7): 781-793.https://doi.org/10.1080/10407782.2015.1090819

[26] Mintsa, H.A., Roy, G., Nguyen, C.T., Doucet, D. (2009). New temperature dependent thermal conductivity data for water-based nanofluids. International Journal of Thermal Sciences, 48(2): 363-371. http://dx.doi.org/10.1016/j.ijthermalsci.2008.03.009

NOMENCLATURE

a	The *flux* (T, ϕ, ω, ψ)
B	uniform magnetic field
b	The power vector of emissivity
D_B	Brownian diffusion coefficient
D_T	Thermophoretic diffusion coefficient
F_{ij}, F_{ik}	The factor of form
H	Cavity height [m]
Ha	Hartman number
h	Heat transfer coefficient [$Wm^{-2}K^{-1}$]
J	The radiosity
L_C	Non-Dimensional polygon closed contour
L_{CI}	Non-Dimensional inner polygon closed contour
L_d	Non-Dimensional parallelogramclosed contour
Le	Lewis number
M	Matrix
Nr	Buoyancyrationumber
N_r	Number of radiation
Nuc	Nusselt number of convection
Nur	Nusselt number of radiative
Nu_t	$Nu_c + Nu_r$
Nb	Brownian motion parameter
Nt	thermophoretic parameter
Pr	Prandtl Number
q_r	Non-dimensional net flux of radiation
Ra	The Rayleigh Number
t	Non-Dimensional time
t^+	Dimensional time [s]
T	Non-Dimensional temperature
T^+	Dimensional temperature [k]
T_0	Average temperature [k]
T_C	Non-Dimensional temperature of cold wall
T_C^+	Dimensional temperature of cold wall [k]
T_H	Non-Dimensional temperature of hot wall
T_H^+	Dimensional temperature hot wall [k]
U, V	Components of non-dimensional velocity
u, v	Components of dimensional velocity [m/s]
X, Y	Non-dimensional cartesian coordinates
x, y	Dimensional cartesian coordinates [m]

Greek symbols

α	The thermal diffusivity [m^2/s]
β	The coefficient of volumetric expansion [K^{-1}]
ΔT	Difference of temperature [K]
ε	The emissivity
κ	Electric conductivity
λ_{nf}	Nanofluid thermal conductivity [$W/(K\,m)$]
μ	The dynamic viscosity
ν	The cinematic viscosity
ρ	The Nanofluid density
$(\rho c)_f$	$\rho_f c_f$
ρ_f	fluid density
c_f	Heat capacity of fluid
$(\rho c)_P$	$\rho_P c_P$
ρ_P	nanoparticles density
c_P	Heat capacity of nanoparticles
σ	The constant of Stefan-Boltzmann
φ	Volume fraction of nanoparticle
φ_c	Volume fraction of nanoparticle at cold wall
φ_h	Volume fraction of nanoparticle at hot wall
ϕ	Non-Dimensional volume fraction of nanoparticle
ψ	Non-Dimensional stream function
ψ^+	Dimensional stream function [m^2/s]
ω	Non-Dimensional vorticity
ω^+	Dimensional vorticity[s^{-1}]